ELSEVIER

Journal of Photochemistry and Photobiology A: Chemistry 107 (1997) 1–8

Journal of PHOTOCHEMISTRY AND PHOTOBIOLOGY A:CHEMISTRY

Branching ratios for the production of the electronic states $BaBr(A^2\Pi_{1/2,3/2}, B^2\Sigma^+)$ from the reaction of $Ba[6s5d(^3D_J)]$ with CH_3Br investigated by time-resolved atomic emission and molecular chemiluminescence following pulsed dye laser excitation of atomic barium

D. Husain [a,*], Jie Lei [a], F. Castaño [b], M.N. Sánchez Rayo [b]

[a] *The Department of Chemistry, The University of Cambridge, Lensfield Road, Cambridge, CB2 1EW, UK*

[b] *Departamento de Quimica Fisica, Universidad del Pais Vasco, Apartado 644, 48080 Bilbao, Spain*

Received 31 October 1996; accepted 2 January 1997

Abstract

We present measurements of the branching ratios for the production of the electronic states $BaBr(A^2\Pi_{1/2,3/2}, B^2\Sigma^+)$ from the reaction of $Ba[6s5d(^3D_J)]$ with CH_3Br investigated by time-resolved atomic emission and molecular chemiluminescence following pulsed dye laser excitation of atomic barium at elevated temperature (900 K). $Ba[6s5d(^3D_J)]$, 1.151 eV above the $6s^2(^1S_0)$ ground state, was generated after the initial pulsed dye laser excitation of atomic barium via the allowed transition at $\lambda = 553.5$ nm ($Ba[6s6p(^1P_1)] \leftarrow Ba[6s^2(^1S_0)]$) in excess helium buffer gas at 900 K. A combination of radiative and collisional processes in excess helium then yielded the optically metastable $Ba(^3D_J)$ state in the "long-time domain". This may be monitored at $\lambda = 791.1$ nm ($Ba[6s6p(^3P_1)] \rightarrow Ba[6s^2(^1S_0)]$), employed as the spectroscopic atomic emission transition. The following long-wavelength molecular chemiluminescence transitions of BaBr were also monitored as a function of time (resulting from the collision of $Ba[6s5d(^3D_J)]$ with CH_3Br): $BaBr(A^2\Pi_{1/2} \rightarrow X^2\Sigma^+, \lambda = 1002$ nm, $\Delta v = 0)$; $BaBr(A^2\Pi_{3/2} \rightarrow X^2\Sigma^+, \lambda = 943$ nm, $\Delta v = 0)$; $BaBr(B^2\Sigma^+ \rightarrow X^2\Sigma^+, \lambda = 883$ nm, $\Delta v = 0)$. These measurements in the time domain, particularly the $A^2\Pi_{1/2} - X^2\Sigma^+$ transition, are feasible using a long-wavelength photomultiplier tube operating in this region. The exponential atomic and molecular profiles are characterized by decay coefficients which are equal in given reactant mixtures, from which it may be concluded that the three molecule states, $BaBr(A^2\Pi_{1/2,3/2}, B^2\Sigma^+)$, are generated directly on collision of $Ba(^3D_J)$ with CH_3Br via exothermic reactions.

The determination of the integrated intensities for the atomic emission and molecular emissions, coupled with optical sensitivity calibrations, yielded branching ratios in the $BaBr(A^2\Pi_{1/2,3/2}, B^2\Sigma^+)$ states, with the following results: $BaBr(A^2\Pi_{1/2})$, 3.80%; $BaBr(A^2\Pi_{3/2})$, 1.69%; $BaBr(B^2\Sigma^+)$, 0.49%. The absolute magnitudes of these branching ratios are comparable with analogous results for the reactions of $Ba(^3D_J)$ with CH_3Cl and CH_3F reported previously. The relative variation of the branching ratios, as seen through their logarithmic variation with the energies of the states, is essentially Boltzmann in character, with an effective temperature close to the ambient temperature of the measurements, indicating the absence of propensity in the yields of these excited molecular states on collision and reflecting the role of late barriers in the potential surfaces involved. © 1997 Elsevier Science S.A.

Keywords: BaBr molecular chemiluminescence; Electronically excited Ba; Electronic branching ratios; Time-resolved atomic emission

1. Introduction

Monitoring of product molecular chemiluminescence in order to study halogen atom abstraction reactions of metastable $Ba[6s5d(^3D_J)]$, 1.151 eV above the $6s^2(^1S_0)$ ground state ($J = 1$, 1.120 eV; $J = 2$, 1.143 eV; $J = 3$, 1.190 eV [1]), has hitherto been carried out in molecular beam systems in which the ^3D_J state has been generated by electric discharge. Reactions of $Ba(^3D_J)$ with Cl and Br halogenated species in beam gas scattering measurements have been reported by Campbell and Dagdigian [2]. Solarz and Johnson [3] have reported measurements on $Ba(^3D_J)$ + halogenated methanes in a molecular beam apparatus, in which atomic barium was initially excited by a pulsed dye laser to $Ba[6s6p(^1P_1)]$, and the ground state diatomic barium halide products resulting from the reaction of the ^3D_J state were then monitored from

* Corresponding author. Tel.: +44 1223 336463

PII S1010-6030(97)00003-8

the $X^2\Sigma^+$ electronic ground state by laser-induced fluorescence. A particularly detailed set of molecular chemiluminescence studies has been presented by Engelke [4] of the reactions of metastable alkaline earth atoms, generated in a molecular beam system by arc discharge, with molecular halogens, including the reaction $Ba(^3D_J) + F_2$. The study of fundamental collisional processes by the generation of metastable electronically excited alkaline earth atoms in molecular beams, especially by low voltage discharge, coupled with atomic emission and molecular chemiluminescence studies on reaction has been reviewed [5–7]. In general, chemical reactions of the low-lying, optically metastable states of Mg, Ca and Sr, involving atom abstraction, have been widely investigated in the time domain, in contrast with the single-collision condition, as the atomic states are directly accessible on pulsed dye laser excitation [8–11]. This can be seen particularly in the study of $Sr[5s5p(^3P_J)]$ with various halide species [12–17] where molecular chemiluminescence has been extensively employed. By contrast, collisional investigation of the low-lying metastable states of atomic barium, namely $Ba[6s5d(^3D_J)]$ and $Ba[6s5d(^1D_2)]$ (1.413 eV [1]), have normally involved the initial use of strong atomic transitions with laser excitation into higher lying short-lived states, followed by a range of collisional and radiative processes eventually leading to the metastable species. $Ba[6s5d(^3D_J)]$ is characterized by a long mean radiative lifetime ($\tau_e \approx 100$ μs to 1 ms or more [3,18]) as is the low-lying $^1D_2$ state (1.413 eV [1]) ($\tau_e(Ba[6s5d(^1D_2)]) \leq 31.3$ μs [19,20]), and these may readily be investigated on timescales far greater than the short-lived states of atomic barium initially excited by pulsed laser methods. Initial excitation of atomic barium has typically involved transitions to $Ba[6s6p(^1P_1)]$ ($\tau_e = 8.37 \pm 0.38$ ns [21]) and $Ba[6s6p(^3P_1)]$ ($\tau_e = 1.2 \pm 0.1$ μs [22–24]).

We have recently developed atomic spectroscopic marker methods for monitoring $Ba(^3D_J)$ in noble gases by employing emission from short-lived atomic states in the "long-time domain", following rapid initial laser excitation via an allowed transition, namely from $Ba(^3P_1)$ and $Ba(^1P_1)$ [25–27]. The former is observed via the transition at $\lambda = 791.1$ nm ($Ba[6s6p(^3P_1)] \rightarrow Ba[6s^2(^1S_0)]$), where the $^3P_1$ state is derived from collisional excitation from $Ba(^3D_J)$, and the latter at $\lambda = 553.5$ nm ($Ba[6s6p(^1P_1)] \rightarrow Ba[6s^2(^1S_0)]$), where the $^1P_1$ state results from $^3D_J + ^3D_J$ energy pooling [25–27]. This method has recently been extended to the study of the reaction between $Ba(^3D_J)$ and CH_3F [28] and CH_3Cl [29]. Whilst both studies involve the monitoring of molecular chemiluminescence from BaF,Cl-($A^2\Pi_{1/2,3/2}$, $B^2\Sigma^+$) in the time domain following halogen atom abstraction, together with time-resolved atomic emission, the procedures are not fully identical [28,29]. This arises because the monitoring of the molecular chemiluminescence from these electronically excited barium halides in the time regime at long wavelength is, firstly, inherently weak as a result of the magnitude of the branching ratios into the molecular excited states on collision. Secondly, the molecular emissions are recorded at particularly long wavelengths, e.g. above 1000 nm in the present investigation involving BaBr, necessarily requiring the use of a new photomultiplier tube [30] operating in this region, where the sensitivity is limited, as expected. The combination of these two effects necessarily limits the form of the kinetic analysis that can be employed as a result of the relatively weak molecular BaF,Cl($A_{1/2,3/2}$, B–X) emission signals [28,29]. Nevertheless, the development and application of this photomultiplier tube have made time-resolved molecular emission measurements feasible in the present context [28–30], where a monochromator must be used at different wavelengths in order to keep the geometry of the optical system constant.

In this paper, we present an investigation of the time-resolved chemiluminescence molecular emission BaBr-($A^2\Pi_{1/2,3/2}$, $B^2\Sigma^+ \rightarrow X^2\Sigma^+$), made at particularly long wavelengths (see below), together with the spectroscopic atomic marker transitions, following the reaction of $Ba(^3D_J)$ with CH_3Br. The measurements are analogous to those described for the investigations in the time domain for $Ca[4s4p(^3P_J)] + CH_3Br$ [31] and $Sr[5s5p(^3P_J)] + CH_3Br$ [13], with the added dimension of integrated atomic and molecular intensity measurements. In the present measurements, a comparison of the time dependences of the atomic and molecular emission profiles demonstrates the direct production of BaBr($A^2\Pi_{1/2,3/2}$, $B^2\Sigma^+$) on reaction. This, together with the measurement of the integrated intensities, yields the branching ratios into these electronically excited molecular states. This distribution is seen to be Boltzmann in character, with no electronic propensity in the product states, indicating late barriers in the appropriate potential surfaces for reaction.

2. Experimental details

The experimental arrangement for monitoring time-resolved atomic emission and molecular chemiluminescence was similar to that reported previously for the kinetic behaviour of $Ba[6s5d(^3D_J)]$ in noble gases [25–27] and of the reactions of $Ba(^3D_J)$ with CH_3F [28] and CH_3Cl [29]. The arrangement is therefore only summarized here with appropriate modifications for studying BaBr in emission, in particular the requirement for measurements at wavelengths longer than those used hitherto in this context [28,29] and the associated experimental constraints arising from limitations in intensity measurements (on a common scale for all emitting species) and their subsequent integration. Initial excitation of ground state atomic barium to $Ba[6s6p(^1P_1)]$ employed a dye laser (rhodamine chloride 590) operating at $\lambda = 553.5$ nm ($Ba[6s6p(^1P_1)] \leftarrow Ba[6s^2(^1S_0)]$), pumped by the second harmonic (532 nm) of a Nd:YAG primary laser (10 Hz) (J.K. Lasers, System 2000). It has previously been established that atomic emission directly from $Ba[6s5d(^3D_1)] \rightarrow Ba[6s^2(^1S_0)]$ at $\lambda = 1106.9$ nm in this type of system using the present long-wavelength photo-

multiplier tube [30], sensitive in this region, cannot be detected directly, even using an interference filter for greater light gathering power [25–27]. Thus Ba(^3D_J) was monitored using the atomic spectroscopic marker from Ba($^3P_1$) at $\lambda = 791.1$ nm following collisional activation of Ba(^3D_J) to the ^3P_J state. The product molecular electronic states resulting from the reaction of Ba(^3D_J) and CH_3Br were monitored by molecular chemiluminescence at long wavelengths in the time domain from the following systems: BaBr($A^2\Pi_{1/2} \rightarrow X^2\Sigma^+$, $\lambda = 1002$ nm, $\Delta v = 0$); BaBr($A^2\Pi_{3/2} \rightarrow X^2\Sigma^+$, $\lambda = 943$ nm, $\Delta v = 0$); BaBr($B^2\Sigma^+ \rightarrow X^2\Sigma^+$, $\lambda = 883$ nm, $\Delta v = 0$).

It can be seen that the photomultiplier–monochromator system, employing the new infrared-sensitive photomultiplier tube (Hamamatsu R632-S1 response) described previously in our investigations on the reactions of Ba(^3D_J) and CH_3F [28] and Ba(^3D_J) and CH_3Cl [29], with a photocathode material of Ag–O–Cs and a sensitivity range of approximately 400–1200 nm, is critical to the measurements at long wavelength, particularly the emission of BaBr($A^2\Pi_{1/2} - X^2\Sigma^+$). The gain of this tube can sensibly be described by the form $\ln G = 8.48 \ln V(\text{volt}) - 47.28$ [30] from the commercial gain characteristic, and this will be employed in the intensity measurements. This was combined with a high throughput compact monochromator operating in the range 350–1100 nm and marginally beyond [30], where the total optical system was calibrated against a spectral radiometer. The photomultiplier was gated electronically against the scattered light from the laser [30]. We must stress that, as in all measurements of this type, the wavelength response of the photomultiplier–monochromator system and the gain characteristic of the photomultiplier tube are employed only in placing the integrated atomic and molecular intensities on a common intensity scale, derived from the decay profiles, and are used in the determination of the branching ratios. The characterization of the time dependences alone of both the atomic and molecular decay profiles is, of course, independent of these calibrations. Digitized data for complete atomic and molecular emission profiles were captured using a double-channel transient digitizer interfaced to a computer; 255 decay profiles were captured and averaged as were 255 background profiles before transfer and subtraction for computerized analysis [25–29]. The materials (Ba (Aldrich Chemicals), He, CH_3Br) were employed essentially as described in the previous time-resolved investigations [13,25–27,31].

3. Results and discussion

3.1. Atomic and molecular decay profiles

Fig. 1 shows examples of the time variation of the digitized output, indicating the exponential decay profiles for Ba(^3D_J) in the "long-time domain" and the associated first-order decay plots derived from the atomic emission at

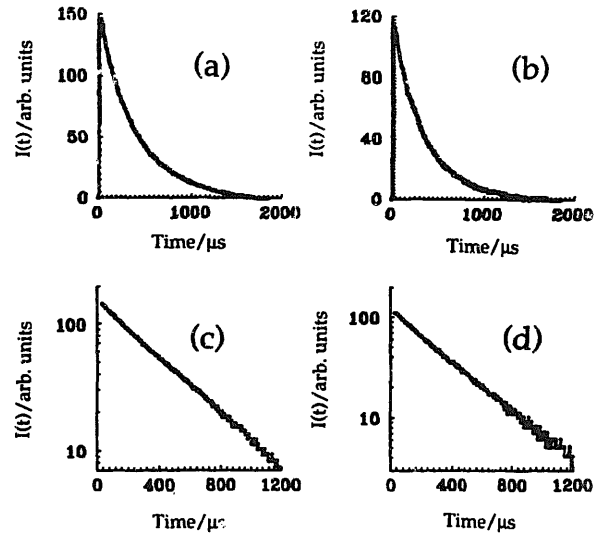

Fig. 1. Examples of the time variation of the exponential decay profiles (a, b) and the associated computerized fitting indicating the first-order decay plots (c, d) for the time-resolved atomic fluorescence emission I_F at $\lambda = 791.1$ nm (Ba[6s6p($^3P_1$)] → Ba[6s^2($^1S_0$)]) following the pulsed dye laser excitation of barium vapour at $\lambda = 553.5$ nm (Ba[6s6p($^1P_1$)] ← Ba[6s^2($^1S_0$)]) in the presence of CH_3Br and excess helium buffer gas ($p_{\text{total with He}} = 80$ Torr) at elevated temperature ($T = 900$ K). [CH_3Br] (10^{15} molecules cm^{-3}): (a, c) 7.3; (b, d) 14.7.

$\lambda = 791.1$ nm (Ba[6s6p($^3P_1$)] → Ba[6s^2($^1S_0$)]) following the pulsed dye laser excitation of barium vapour at 900 K [32] at $\lambda = 553.5$ nm (Ba[6s6p($^1P_1$)] ← Ba[6s^2($^1S_0$)]) in the presence of CH_3Br and excess helium buffer gas. The use of this spectroscopic marker method for monitoring the time variation of Ba(^3D_J) following the initial pulsed dye laser excitation of atomic barium to Ba[6s6p($^1P_1$)] has been demonstrated in earlier investigations [25–27]. This is established using the rate constants for the processes of collisional activation

$$\text{Ba}[6s5d(^3D_J)] + \text{He} \rightarrow \text{Ba}[6s6p(^3P_J)] + \text{He} \quad k_1^{\text{He}} \qquad (1)$$

$$\text{Ba}[6s5d(^3D_J)] + \text{Ba} \rightarrow \text{Ba}[6s6p(^3P_J)] + \text{Ba} \quad k_2^{\text{Ba}} \qquad (2)$$

calculated by employing the rate data reported for the reverse of processes (1) and (2) for the collisional relaxation of Ba(^3P_J) by He and Ba($^1S_0$) to Ba(^3D_J) given by Kallenbach and Koch [33,34] using the principle of detailed balance [25–27]. The decay of Ba(^3D_J) may be expressed in the form

$$\text{Ba}[6s5d(^3D_J)]_t = \text{Ba}[6s5d(^3D_J)]_{t=0} \exp(-k't) \qquad (i)$$

where the first-order decay coefficients k' are derived from the slopes of the plots of the type given in Fig. 1(c) and 1(d) and include the collisional removal by CH_3Br. The first-order decay coefficient for Ba(^3D_J) can then be written as

$$k' = k'_{\text{em}} + \beta/p_{\text{He}} + \Sigma k_Q[Q] + k_R[CH_3Br] \qquad (ii)$$

where the symbols have their usual significance [25–29]. The removal of Ba(^3D_J) is assumed, as previously, to be dominated by chemical reaction to yield BaBr (see below), and will be the basis of the estimation of an upper limit for

the branching ratio into the ground state BaBr($X^2\Sigma^+$). It must be stressed that, as in previous measurements of this kind [28,29] and, mutatis mutandis, analogous measurements on halogen atom abstraction reactions by $Sr(5^3P_J)$ [14–17], this is the only consequence of this type of assumption, recognizing that there may be a contribution from collisional quenching of $Ba(^3D_J)$ to $Ba(^1S_0)$. This does not affect the time dependence in the kinetic analysis of either the atomic or molecular decay and their comparison, nor the determination of the branching ratios into the electronically excited states BaBr($A^2\Pi_{1,2/3/2}$, $B^2\Sigma^+$).

k'_{cm} is given by the form [25–27]

$$k'_{cm} = A_{nm}/(1 + K_1 + K_1K_2) \qquad \text{(iii)}$$

where emission from the ^3D_J state will be dominated by electric-dipole-allowed radiation from $Ba[6s5d(^3D_1)]$ in (jj) coupling and A_{nm} is the Einstein coefficient for the transition $^3D_1 \rightarrow {}^1S_0$. Rapid Boltzmann equilibration between the ^3D_J levels will have taken place in the long-time regime [35] leading to Eq. (iii), and the equilibrium constants connecting these spin–orbit states are written as $^3D_1 \rightleftharpoons {}^3D_2$ ($\Delta\epsilon = 182$ cm^{-1} [1,35]) (K_1) and $^3D_2 \rightleftharpoons {}^3D_3$ ($\Delta\epsilon = 381$ cm^{-1} [1,35]) (K_2), and may readily be calculated by statistical thermodynamics. The function $F = (1 + K_1 + K_1K_2)$ takes a value of 3.18 in the present measurements (900 K), and reaches a value of 5 at infinite temperature, where it is solely dependent on the statistical weights of the spin–orbit components. The term β/p_{He} describes the diffusional loss of $Ba(^3D_J)$ and is negligible in relation to other kinetic loss processes in this type of system above pressures of helium greater than approximately 30 Torr [25–27], the main gas present in these measurements. More importantly in the present system, where measurements were taken at $p_{He} = 80$ Torr, is that its contribution is constant. The term $\Sigma k_Q[Q]$ includes the collisional removal of $Ba(^3D_J)$ by He which is small [25] and by ground state $Ba(^1S_0)$ itself in the form $k_{Ba}[Ba]$. k_{Ba} has been characterized using the present method [25–27] and in other measurements [36–38] and, again, the term $k_{Ba}[Ba]$ is constant in this system where measurements were carried out at constant temperature (900 K) and hence a constant vapour density of $Ba(^1S_0)$. The term k_R includes all collisional removal of $Ba(^3D_J)$ by CH_3Br and is described by various exothermic chemical reactions to yield BaBr in various accessible electronic states, including the ground state. The intensity of the atomic emission arising from collisional excitation from $Ba(^3D_J)$ to $Ba[6s6p(^3P_1)]$, and its time dependence, will take the form [25–29]

$$I_{cm}(791.1\text{ nm}) = GS(k_1^{He}[He] + k_2^{Ba}[Ba])Ba[6s5d(^3D_J)]_{t=0}\exp(-k't) \qquad \text{(iv)}$$

where G is the gain of the photomultiplier, which is a function of the voltage, and S is the sensitivity of the optical system, calibrated as indicated. All emission intensities are, of course, normalized to a common relative scale (see Section 2). In the kinetic analysis presented later, the symbols involving G and S are not given in the presentation for simplicity, but are, of course, included in the analysis involving integrated intensity measurements.

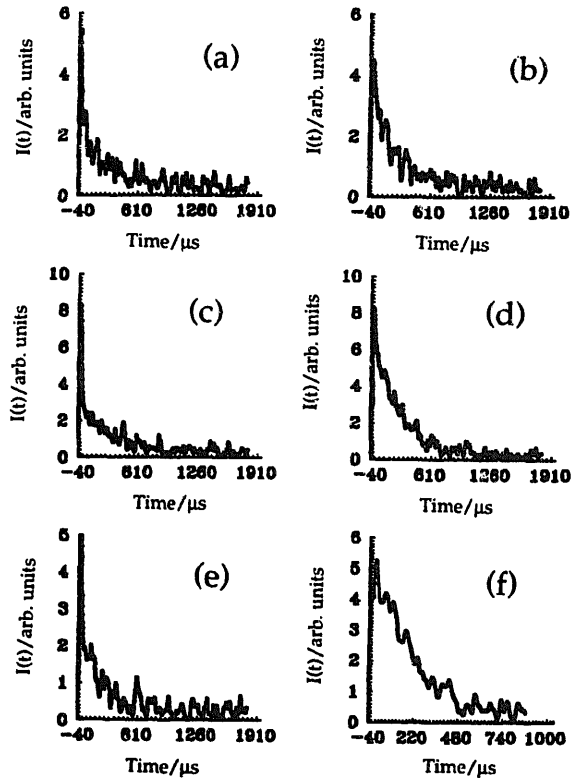

Fig. 2. Examples of the time variation of the digitized output indicating the decay profiles for the time-resolved molecular chemiluminescence from BaBr($A^2\Pi_{1/2} \rightarrow X^2\Sigma^+$, $\lambda = 1002$ nm, $\Delta v = 0$) (a,b), BaBr($A^2\Pi_{3/2} \rightarrow X^2\Sigma^+$, $\lambda = 943$ nm, $\Delta v = 0$) (c,d) and BaBr($B^2\Sigma^+ \rightarrow X^2\Sigma^+$, $\lambda = 883$ nm, $\Delta v = 0$) (e,f) following the pulsed dye laser excitation of barium vapour at $\lambda = 553.5$ nm ($Ba[6s6p(^1P_1)] \leftarrow Ba[6s^2(^1S_0)]$) in the presence of CH_3Br and excess helium buffer gas ($p_{total\ with\ He} = 80$ Torr) at elevated temperature ($T = 900$ K). [CH_3Br] (10^{15} molecules cm^{-3}): (a, c, e) 7.3; (b, d, f) 14.7.

Fig. 2 shows examples of the time variation of the digitized output, indicating the decay profiles for the time-resolved molecular chemiluminescence from BaBr($A^2\Pi_{1/2} \rightarrow X^2\Sigma^+$, $\lambda = 1002$ nm, $\Delta v = 0$), BaBr($A^2\Pi_{3/2} \rightarrow X^2\Sigma^+$, $\lambda = 943$ nm, $\Delta v = 0$) and BaBr($B^2\Sigma^+ \rightarrow X^2\Sigma^+$, $\lambda = 883$ nm, $\Delta v = 0$) following the pulsed dye laser excitation of barium vapour at the resonance wavelength of $\lambda = 553.5$ nm in the presence of CH_3Br and excess helium buffer gas under conditions identical to those indicated in Fig. 1 for the atomic profiles. At these long wavelengths, the molecular emission signals are particularly weak, as indicated earlier, due to the combination of the relatively low sensitivity of the photomultiplier tube (R632, see Section 2) and the low branching ratios into the electronically excited molecular states. Thus whilst some first-order decay profiles for the molecular emissions will be presented, and will demonstrate scatter, as expected, these are constructed from direct exponential fitting to the raw profiles of the type shown in Fig. 2, as are the integrated molecular intensities. Figs. 3 and 4 thus show first-order decay plots for the molecular emissions from BaBr($A^2\Pi_{1/2}$

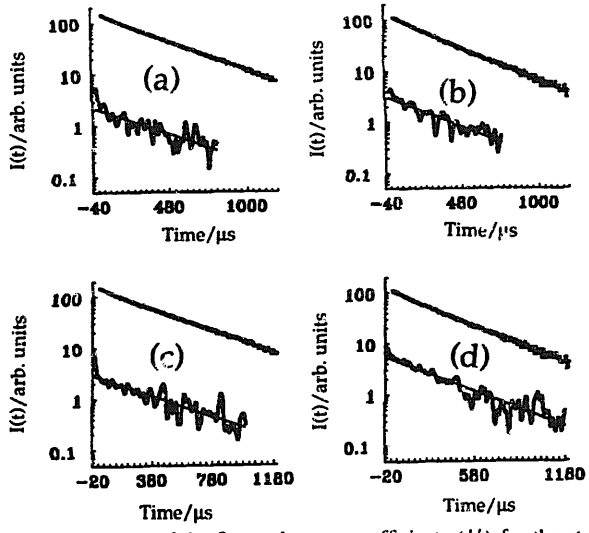

Fig. 3. Comparison of the first-order rate coefficients (k') for the atomic fluorescence derived from the intensity profiles for the Ba[6s6p($^1P_1$)] → Ba[6s^2($^1S_0$)] emission at $\lambda = 791.1$ nm with those of the molecular chemiluminescence for the BaBr($A^2\Pi_{1/2} \rightarrow X^2\Sigma^+$) emission at $\lambda = 1002$ nm (a,b) and BaBr($A^2\Pi_{3/2} \rightarrow X^2\Sigma^+$) emission at $\lambda = 943$ nm (c,d) following the pulsed dye laser excitation of barium vapour at $\lambda = 553.5$ nm (Ba[6s6p($^1P_1$)] ← Ba[6s^2($^1S_0$)]) in the presence of CH_3Br and excess helium buffer gas ($p_{\text{total with He}} = 80$ Torr) at elevated temperature ($T = 900$ K) (top line, atomic emission; bottom line, molecular emission). [CH_3Br] (10^{15} molecules cm^{-3}): (a, c) 7.3; (b, d) 14.7. (a) $k'_{1002}/k'_{791} = 1.09$; (b) $k'_{1002}/k'_{791} = 1.06$; (c) $k'_{943}/k'_{791} = 1.07$; (d) $k'_{943}/k_{791} = 1.07$.

$\rightarrow X^2\Sigma^+$, $\lambda = 1002$ nm, $\Delta v = 0$), BaBr($A^2\Pi_{3/2} \rightarrow X^2\Sigma^+$, $\lambda = 943$ nm, $\Delta v = 0$) and BaBr($B^2\Sigma^+ \rightarrow X^2\Sigma^+$, $\lambda = 883$ nm, $\Delta v = 0$) and those of the first-order decay profiles for the atomic emissions at $\lambda = 791.1$ nm from Ba[6s6p($^3P_1$)] → Ba[6s^2($^1S_0$)] taken under identical conditions, demonstrating the first-order kinetic decay of Ba(^3D_J). A comparison of the molecular and atomic first-order decay coefficients shows that these are equal to within ±10% as is generally observed here. The error arises primarily from the scatter in the molecular signals.

3.2. Kinetic analysis

The $A^2\Pi_{1/2}$, $A^2\Pi_{3/2}$ and $B^2\Sigma^+$ states of BaBr are thermodynamically accessible on collision between Ba(^3D_J) and CH_3Br as the reaction is highly exothermic [1,39–42]

	ΔH/kJ mol^{-1}		
Ba(^3D_J) + CH_3Br ---> BaBr($X^2\Sigma^+$) + CH_3	-183.9	(3)	k_3
Ba(^3D_J) + CH_3Br ---> BaBr($A^2\Pi_{1/2}$) + CH_3	-64.4	(4)	k_4
Ba(^3D_J) + CH_3Br ---> BaBr($A^2\Pi_{3/2}$) + CH_3	-56.9	(5)	k_5
Ba(^3D_J) + CH_3Br ---> BaBr($B^2\Sigma^+$) + CH_3	-48.3	(6)	k_6

The low-lying $A'^2\Delta$ state ($T_e = 88\,996$ cm^{-1} [43]) of BaBr is optically metastable and the $C^2\Pi_{1/2,3/2}$ state is not energetically accessible [39]. For the electronically excited states which are observed in chemiluminescence, the following vibrational levels are accessible as can be seen from the spectroscopic data [39,42] for these states: $A^2\Pi_{1/2}(v' \leq 32)$, $A^2\Pi_{3/2}(v' \leq 28)$, $B^2\Sigma^+(v' \leq 24)$. The data for the electronic ground state are also listed here for the purpose of Franck–Condon calculations: $X^2\Sigma^+$, $\omega_e = 192.3$ and $\omega_e x_e = 0.41$ cm^{-1}, $r_e = 0.2847$ nm; $A^2\Pi_{1/2,3/2}$, $\omega'_e = 177.13$ and $\omega'_e x'_e = 0.40$ cm^{-1}, $r_e = 0.2899$ nm; $B^2\Sigma^+$, $\omega'_e = 176.60$ and $\omega'_e x'_e = 0.41$ cm^{-1}, $r_e = 0.2898$ nm. The interatomic distances in the $A^2\Pi_{1/2,3/2}$ states are estimated following the measurements of Launila and Royen [42]. Franck–Condon factors were calculated using a simplified Morse oscillator model following Tuckett [44], yielding the following examples: A–X, (0,0) 0.6903, (1,0) 0.2598, (1,1) 0.2719, (0,1) 0.2156; B–X, (0,0) 0.6975, (1,0) 0.2544, (1,1) 0.2834, (0,1) 0.2472. Thus whilst the main emission in the $v = 0$ sequences arises from the $\Delta v = 0$ transitions, off-diagonal terms play a larger role than in analogous studies on emission from strontium halides derived from Sr(5^3P_J) [14–17].

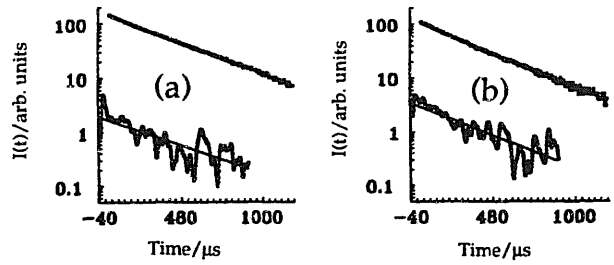

Fig. 4. Comparison of the first-order rate coefficients (k') for the atomic fluorescence derived from the intensity profiles for the Ba[6s6p($^3P_1$)] → Ba[6s^2($^1S_0$)] emission at $\lambda = 791.1$ nm with those of the molecular chemiluminescence for the BaBr($B^2\Sigma^+ \rightarrow X^2\Sigma^+$, $\lambda = 883$ nm, $\Delta v = 0$) emission following the pulsed dye laser excitation of barium vapour at $\lambda = 553.5$ nm (Ba[6s6p($^1P_1$)] ← Ba[6s^2($^1S_0$)]) in the presence of CH_3Br and excess helium buffer gas ($p_{\text{total with He}} = 80$ Torr) at elevated temperature ($T = 900$ K) (top line, atomic emission; bottom line, molecular emission). [CH_3Br] (10^{15} molecules cm^{-3}): (a) 7.3; (b) 14.7. (a) $k'_{883}/k'_{791} = 1.06$; (b) $k'_{883}/k'_{791} = 0.97$.

To the best of our knowledge, of the emitting states monitored in this investigation, only BaBr($B^2\Sigma^+$) has had its mean radiative lifetime characterized (τ_e(B–X) = 123.2 ns [45]), presumably, in part, on account of the constraints imposed by measurements at longer wavelength for emission from the $A^2\Pi$ states of this molecule. The mean radiative lifetimes (τ_e) of the $A^2\Pi$ states of BaCl and BaF have been measured by Berg et al. [46,47] (109.8 and 46.1 ns respectively). We assume that those of the $A^2\Pi_{1/2,3/2}$ states of BaBr are comparably short, and that the $A^2\Pi_{1/2}$, $A^2\Pi_{3/2}$ and $B^2\Sigma^+$ states can be placed in steady state. Considering BaBr($A^2\Pi_{1/2}$) as an example, its concentration may readily be placed in steady state, namely

$$d[\text{BaBr}(A_{1/2})]/dt = k_4[\text{Ba}^3\text{D}]_t[\text{CH}_3\text{Br}] - A'_{nm}[\text{BaBr}(A_{1/2})] = 0 \quad \text{(v)}$$

where $A'_{nm} = 1/\tau_e$ for BaBr($A_{1/2}$). Combining Eq. (v) with Eq. (i), we readily see that, on this basis, the $A_{1/2}$–X emission intensity follows the form

$$I(\text{A}-\text{X}) = k_4[\text{CH}_3\text{Br}][\text{Ba}[6s5d(^3D_J)]]_{t=0}\exp(-k't) \quad \text{(vi)}$$

where the appropriate values of G and S are included later in the integrated intensity calculations. Thus, following Eqs. (iv) and (vi), the molecular and atomic ($\lambda = 791.1$ nm) intensities should both follow the same exponential form for the production of the $A_{1/2}$, $A_{3/2}$ and B states of BaBr resulting from direct reaction, as indicated in processes (4)–(6) and demonstrated in Figs. 3 and 4.

3.3. Branching ratios

Branching ratios into the specific electronic states of BaBr, which describe the rate of production of a given electronic state on reaction with CH_3Br relative to the total removal of $Ba(^3D_J)$ on collision with this molecule, may be characterized in this study. Thus, in the case of $BaBr(A^2\Pi_{1/2})$, this may be considered as k_4/k_R or $k_{A_{1/2}}/k_R$ where k_R represents the overall removal of $Ba(^3D_J)$ by CH_3Br. We have stressed earlier that this could include collisional quenching of $Ba(^3D_J)$ to the $^1S_0$ ground state, where the assumption of total chemical removal only affects the final estimate of the branching ratio in the $X^2\Sigma^+$ ground state. We first consider the atomic intensity at $\lambda = 791.1$ nm (Eq. (iv)), appropriately normalized via the relevant values of G and S from the intensity calibration. Writing $k_1^{He}[He] + k_2^{Ba}[Ba] = k'_{tr}$, we may integrate Eq. (iv) and obtain

$$I_{^3P} = \int_0^\infty I_{em}(791.1\text{ nm}) = k'_{tr}[Ba(^3D_J)]_{t=0}/k' \qquad \text{(vii)}$$

We have seen earlier that the rate processes (1) and (2) for the activation of $Ba(^3P_1)$ from $Ba(^3D_J)$ may be characterized using the principle of detailed balance and the collisional relaxation rate data for $Ba(^3P_J)$ of Kallenbach and Koch [33,34]. This has been shown to yield the following results: $k_1^{He}(900\text{ K}) = 1.2\times10^{-16}$ cm^3 atoms^{-1} s^{-1} and $k_2^{Ba}(900\text{ K}) = 1.0\times10^{-11}$ cm^3 atoms^{-1} s^{-1} [25–27]. Thus for $p_{He} = 80$ Torr and a temperature of 900 K, where $[Ba] = 6.15\times10^{13}$ atoms cm^{-3} from vapour pressure data [32], k'_{tr} may be calculated and takes the value of 722 s^{-1} for this temperature and pressure of helium.

For the example of $BaBr(A^2\Pi_{1/2})$, we may integrate Eq. (vi), namely

$$I_{A_{1/2}} = \int_0^\infty I_{em}(1002\text{ nm}) = k_4[CH_3Br][Ba(^3D_J)]_{t=0}/k' \qquad \text{(viii)}$$

where $I_{em}(1002\text{ nm}) = I(A\text{–}X)$. Following Eqs. (ii) and (iv), we may plot k' for $Ba(^3D_J)$ vs. $[CH_3Br]$ using the emission at $\lambda = 791.1$ nm (Fig. 5) and obtain the value of k_R from the slope ($S(I)$). This plot is scattered, principally in view of the removal of CH_3Br by barium metal itself at the surface at elevated temperature before reaching the reactor (see below). Furthermore, by combining Eqs. (vii) and (viii), we see that

$$I_{A_{1/2}}/I_{^3P} = k_4[CH_3Br]/k'_{tr} \qquad \text{(ix)}$$

Thus a plot of $I_{A_{1/2}}/I_{^3P}$ from the calibrated molecular and atomic integrated intensities vs. $[CH_3Br]$ has a slope ($S(II)$) of k_4/k'_{tr}. Hence, $S(II)/S(I) = k_4/k_Rk'_{tr}$ or $k_{A_{1/2}}/k_Rk'_{tr}$, yielding the branching ratio into $BaBr(A^2\Pi_{1/2})$. Relevant plots of $I_{A_{1/2}}/I_{^3P}$, $I_{A_{3/2}}/I_{^3P}$ and $I_B/I_{^3P}$ vs. $[CH_3Br]$ are given in Fig. 6(a), (b) and (c) respectively. These plots are scattered as the intensities of the molecular emissions are weak, arising from the use of the long-wavelength photomultiplier tube at

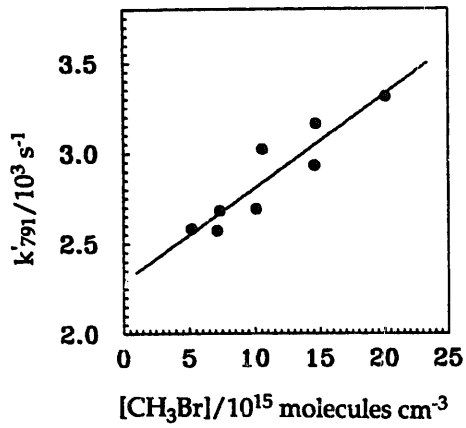

Fig. 5. Variation of the pseudo-first-order rate coefficient $k'_{791}(^3P_1)$ for the decay of $Ba[6s6p(^3P_1)]$ generated by energy transfer from $Ba[6s5d(^3D_J)]$ in the presence of varying concentrations of CH_3Br and excess helium buffer gas ($p_{total\ with\ He} = 80$ Torr) at elevated temperature ($T = 900$ K) following the pulsed dye laser excitation of barium vapour at $\lambda = 553.5$ nm ($Ba[6s6p(^1P_1)] \leftarrow Ba[6s^2(^1S_0)]$).

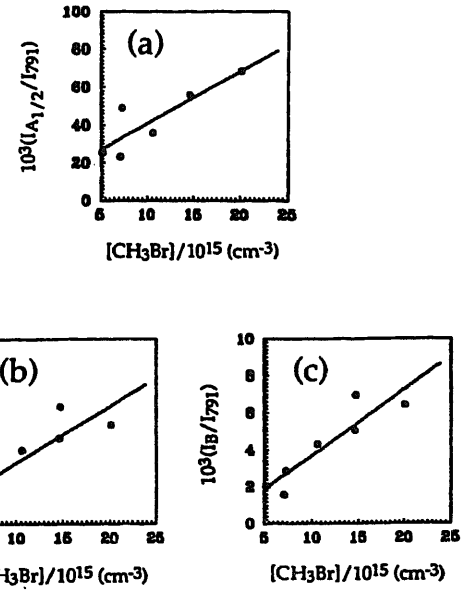

Fig. 6. Variation of the integrated intensity ratios for the molecular chemiluminescence emission to the atomic fluorescence emission $Ba[6s6p(^3P_1)] \rightarrow Ba[6s^2(^1S_0)]$ at $\lambda = 791.1$ nm and the concentration of CH_3Br following the pulsed dye laser excitation of barium vapour at $\lambda = 553.5$ nm ($Ba[6s6p(^1P_1)] \leftarrow Ba[6s^2(^1S_0)]$) in the presence of CH_3Br and excess helium buffer gas ($p_{total\ with\ He} = 80$ Torr) at elevated temperature ($T = 900$ K). Molecular chemiluminescence emission: (a) $BaBr(A^2\Pi_{1/2} \rightarrow X^2\Sigma^+$, $\lambda = 1002$ nm, $\Delta v = 0$); (b) $BaBr(A^2\Pi_{3/2} \rightarrow X^2\Sigma^+$, $\lambda = 943$ nm, $\Delta v = 0$); (c) $BaBr(B^2\Sigma^+ \rightarrow X^2\Sigma^+$, $\lambda = 883$ nm, $\Delta v = 0$).

long wavelength where its sensitivity is relatively low, coupled with the low overall sensitivity of the tube and the low branching ratios into the electronic states. This then involves the use of increased gain in the photomultiplier tube with an accompanying increase in noise. We may also note that the inclusion of a factor f in Eq. (ii) (via Fig. 5) and Eq. (ix) to allow for the removal of a certain proportion of CH_3Br before reaching the centre of the reactor prior to laser excitation, writing the effective reactant concentration as $f[CH_3Br]$, will cancel. Indeed, the present method only depends on the use of identical concentrations of CH_3Br when recording the atomic and molecular decay profiles in a given measurement. An alternative approach has been employed hitherto [28] using a given concentration of $[CH_3F]$ to determine the branching ratios into the electronic states of BaF with the analogue of Eq. (ix), coupled with $S(I)$, point by point, where plots such as those in Fig. 6 could not be constructed as a result of large scatter. In the present case, Eq. (ix) and Fig. 6 were used to determine the following branching ratios: $BaBr(A^2\Pi_{1/2})$, 3.80%; $BaBr(A^2\Pi_{3/2})$, 1.69%; $BaBr(B^2\Sigma^+)$, 0.49%. These results may be compared with the branching ratios for the reaction of $Ba(^3D_J)$ with CH_3Cl ($BaCl(A^2\Pi_{1/2})$, 4.68%; $BaCl(A^2\Pi_{3/2})$, 1.29%; $BaCl(B^2\Sigma^+)$, 0.24% [29]) and for the reaction of $Ba(^3D_J)$ with CH_3F ($BaF(A^2\Pi_{1/2})$, 0.86%; $BaF(A^2\Pi_{3/2})$, 0.42%; $BaF(B^2\Sigma^+)$, 0.05% [28]).

These branching ratios are of comparable magnitude with those reported hitherto for the production of various diatomic strontium halides in the $A^2\Pi_{1/2,3/2}$, $B^2\Sigma^+$ states following reactions of $Sr(5^3P_J)$ with halogenated species [14–17] in pulsed dye laser measurements where $Sr(5^3P_1)$ was directly populated on laser excitation. Plots of the logarithm of the branching ratios from the reactions of $Ba(^3D_J)$ with CH_3Br, CH_3Cl and CH_3F into BaBr,Cl,F($A^2\Pi_{1/2,3/2}$, $B^2\Sigma^+$) vs. the energy of the states of BaBr, BaCl and BaF are sensibly linear (Fig. 7). The slope of the plot for CH_3Br yields an effective temperature of approximately 970 K compared with that for CH_3Cl of about 730 K and that for CH_3F of approximately 1200 K, all of which may be compared with the ambient temperature in all the measurements of 900 K. It must be stressed that the measurements were made over a limited range of electronic energies for the states of BaBr, BaCl and BaF. Furthermore, comparison of the calibrated atomic and molecular intensities shows a variation of up to a factor of approximately 10^4 in some cases, especially for the long-wavelength molecular transitions. Thus we conclude that the effective temperatures in the plots in Fig. 7 are sensibly in accord with the ambient temperature. Assuming that the removal of $Ba(^3D_J)$ by CH_3Br results only in the formation of BaBr and not in physical quenching to yield $Ba(^1S_0)$ (see earlier), this yields an upper limit for the branching ratio into $BaBr(X^2\Sigma^+)$ of about 94%, a result similar to that found for $BaCl(X^2\Sigma^+)$ [29]. The analogous upper limit for $BaF(X^2\Sigma^+)$ was found to be approximately 99% [28]. The absolute values for the branching ratios are influenced by the magnitude of k'_{tr}, namely by the collisional activation rates

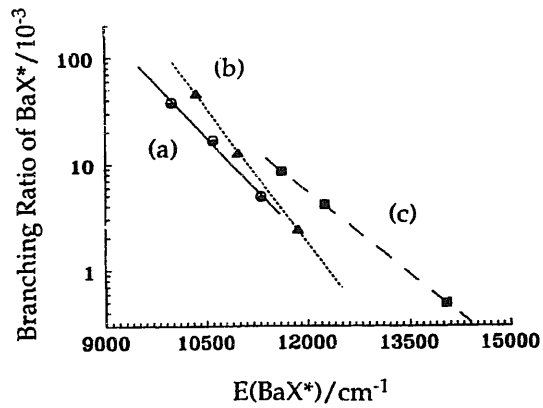

Fig. 7. Variation of the branching ratios into electronically excited BaBr, BaCl and BaF (BaX: $A^2\Pi_{1/2}$, $A^2\Pi_{3/2}$, $B^2\Sigma^+$), observed by time-resolved chemiluminescence after halogen atom abstraction reactions of $Ba[6s5d(^3D_J)]$ with CH_3Br (a), CH_3Cl (b) and CH_3F (c) following the pulsed dye laser excitation of barium vapour at elevated temperature as a function of the electronic energy of the state.

of $Ba(^3D_J)$ into $Ba(^3P_J)$ by Ba and He [33,34] as described earlier. The relative branching ratios are not influenced by k'_{tr} and neither is the sensible linearity of the effective Boltzmann plot of the logarithm of the branching ratio vs. the energy of the state of BaBr and the resulting effective temperature. As observed previously for halogen atom abstraction reactions by $Sr(5^3P_J)$ [14–17], this yields the important fundamental conclusion that there is no propensity in the production of the electronically excited states of BaBr on collision of $Ba(^3D_J)$ with CH_3Br, nor for those of BaCl and BaF on collision of $Ba(^3D_J)$ with CH_3Cl and CH_3F [28,29], as seen via the branching ratios; rather, the yields of the molecular states are statistical in nature, presumably reflecting late barriers in the appropriate potential surfaces describing the reactions.

Acknowledgements

We thank the Cambridge Overseas Scholarship Trustees for a Research Studentship held by J.L. during the tenure of which this work was carried out. J.L. also thanks the O.R.S. for an award. Finally, we are indebted to Dr. G.A. Jones of the DRA (Fort Halstead) for encouragement and helpful discussions.

References

[1] C.E. Moore (Ed.), Atomic Energy Levels, Nat. Bur. Stand. Ref. Data Ser., Nat. Bur. Stand. Monograph 35, vols. I–III, US Government Printing Office, Washington DC, 1971.
[2] M.L. Campbell, P.J. Dagdigian, J. Chem. Phys. 85 (1996) 4453.
[3] R.W. Solarz, S.A. Johnson, J. Chem. Phys. 70 (1979) 359...
[4] F. Engelke, Chem. Phys. 39 (1979) 279; 44 (1979) 213.
[5] I.M. Campbell, P.J. Dagdigian, Chem. Rev. 87 (1987) 1; Faraday. Discuss. Chem. Soc. 84 (1987) 127.
[6] H.F. Davis, S.G. Suily, Y.T. Lee, in: .. Fontijn (Ed.), Gas Phase Metal Reactions, North Holland, Amsterdam, 1992, Chapter 16, p. 319.

[7] M. Menzinger, in: A. Fontijn (Ed.), Gas Phase Chemiluminescence and Chemi-ionization, North Holland, Amsterdam, 1985, Chapter 3, p. 25.
[8] W.H. Breckenridge, J. Phys. Chem. 100 (1996) 1480.
[9] W.H. Breckenridge, H. Umemoto, in: A. Fontijn, M.A.A. Clyne (Eds.), Reactions of Small Transient Species; Kinetics and Energetics, Academic Press, London, 1983, Chapter 4, p. 157.
[10] D. Husain, G. Roberts, in: J.E. Baggott, M.N.R. Ashfold (Eds.), Bimolecular Collisions, Royal Society of Chemistry Publications, London, 1989, Chapter 6, p. 263.
[11] D. Husain, J. Chem. Soc., Faraday Trans. 2 85 (1989) 8.
[12] M.N. Sánchez Rayo, F. Castaño, M.T. Martinez, J.W. Adams, S.A. Carl, D. Husain, J. Schifino, J. Chem. Soc., Faraday Trans. II 89 (1993) 1645.
[13] F. Castaño, M.N. Sanchez Rayo, R. Peirera, J.W. Adams, D. Husain, J. Schifino, J. Photochem. Photobiol. A: Chem. 83 (1994) 79.
[14] S. Antrobus, D. Husain, J. Lei, F. Castaño, M.N. Sánchez Rayo, Int. J. Chem. Kinet. 27 (1995) 741.
[15] S. Antrobus, D. Husain, J. Lei, F. Castaño, M.N. Sánchez Rayo, J. Chem. Res. (S) 84, (M) 0601 (1995).
[16] S. Antrobus, D. Husain, J. Lei, F. Castaño, M.N. Sánchez Rayo, Z. Phys. Chem. 190 (1995) 267.
[17] S. Antrobus, D. Husain, J. Lei, F. Castaño, M.N. Sánchez Rayo, Laser Chem. 16 (1995) 121.
[18] S.G. Schmelling, Phys. Rev. A 9 (1974) 1097.
[19] J.D. Eversole, N. Djeu, J. Chem. Phys. 71 (1979) 148.
[20] D. Husain, G. Roberts, Chem. Phys. 127 (1988) 203.
[21] S. Niggli, M.C.E. Huber, Phys. Rev. A 35 (1987) 2908.
[22] C.W. Bauschlicher Jr., R.L. Jaffe, S.R. Langhoff, F.G. Mascarello, H. Partridge, J. Phys. B 18 (1985) 2147.
[23] J. Reader, C.H. Corliss, W.L. Wiese, G.A. Martin, Wavelengths and Transition Probabilities for Atoms and Atomic Ions, Nat. Bur. Stand. Ref. Data Ser., Nat. Bur. Stand. Monograph 68, US Government Printing Office, Washington DC, 1980, p. 367.
[24] B.M. Miles, W.L. Wiese, Critically Evaluated Transition Probabilities for Ba I and II, Nat. Bur. Stand. Technical Note 474, US Government Printing Office, Washington DC, 1969.
[25] S. Antrobus, D. Husain, J. Lei, J. Photochem. Photobiol. A: Chem. in press.
[26] S. Antrobus, D. Husain, J. Lei, J. Photochem. Photobiol. A: Chem. in press.
[27] S. Antrobus, D. Husain, J. Lei, Anal. Quim. 92 (1996) 17.
[28] D. Husain, J. Lei, F. Castaño, M.N. Sánchez Rayo, Anal. Quim. in press.
[29] D. Husain, J. Lei, F. Castaño, M.N. Sánchez Rayo, Laser Chem., 17 (1997) 53.
[30] S. Antrobus, D. Husain, J. Lei, J. Photochem. Photobiol. A: Chem. 90 (1995) 1.
[31] F. Beitia, F. Castaño, M.N. Sánchez Rayo, S.A. Carl, D. Husain, L. Santos, Z. Phys. Chem. 171 (1991) 137.
[32] C.B. Alcock, V.P. Itkin, M.K. Harrigan, Can. Met. Q. 23 (1984) 309.
[33] A. Kallenbach, M. Koch, J. Phys. B, At. Mol. Phys. 22 (1989) 1691.
[34] A. Kallenbach, M. Koch, J. Phys. B, At. Mol. Phys. 22 (1989) 1705.
[35] E. Ehrlacher, J. Huennekens, Phys. Rev. A 50 (1994) 4786.
[36] P.G. Whitkop, J.R. Wiesenfeld, J. Chem. Phys. 72 (1980) 1297.
[37] J.L. Carlsten, J. Phys. B, At. Mol. Phys. 7 (1974) 1620.
[38] C. Vadla, K. Niemax, V. Horatic, R. Beuc, Z. Phys. D 34 (1995) 171.
[39] K.P. Huber, G. Herzberg, Molecular Spectra and Molecular Structure. IV. Constants of Diatomic Molecules, Van Nostrand Reinhold, New York, 1979.
[40] B. Rosen, Spectroscopic Data Relative to Diatomic Molecules, Pergamon, Oxford, 1970.
[41] D.R. Lide (Ed.), CRC Handbook of Chemistry and Physics, 75th Edn., CRC Press, Boca Raton, FL, 1994/1995, pp. 9–66.
[42] O. Launila, P. Royen, Mol. Phys. 82 (1994) 815.
[43] A.R. Allouche, G. Wannous, M. Aubert-Frecon, Chem. Phys. 170 (1993) 11.
[44] R.P. Tuckett, personal communication, 1992.
[45] L.-E. Berg, K. Ekvall, E. Hedin, A. Hishikawa, A. Karawajczyk, S. Kelley, T. Olsson, Chem. Phys. Lett. 209 (1993) 47.
[46] L.-E. Berg, A. Hishikawa, A. Karawajczyk, T. Olsson, J. Mol. Spectrosc. 160 (1993) 593.
[47] L.-E. Berg, T. Olsson, J.-C. Chanteloup, A. Hishikawa, P. Royen, Mol. Phys. 79 (1993) 721.